

Diffraction Radiation Diagnostics for Moderate to High Energy Charged Particle Beams

Abstract

Diffraction radiation (DR) is produced when a charged particle passes through an aperture or near a discontinuity in the media in which it is traveling. DR is closely related to transition radiation (TR), which is produced when a charged particle traverses the boundary between media with different dielectric constants. In contrast to TR, which is now extensively used for beam diagnostic purposes, the potential of DR as a non-interceptive, multi-parameter beam diagnostic remains largely undeveloped. For diagnostic measurements it is useful to observe backward reflected DR from a circular aperture or slit inclined with respect to the beam velocity. However, up to now, well founded equations for the spectral-angular intensities of backward DR from such apertures have not been available. We present a new derivation of the spectral angular intensity of backward DR produced from an inclined slit for two orientations of the slit axis, i.e. perpendicular and parallel to the plane of incidence. Our mathematical approach is generally applicable to any geometry and simpler than the Wiener Hopf method previously used to calculate DR from single edges. Our results for the slit are applied to the measurement of orthogonal beam size and divergence components. We discuss the problem of separating the simultaneous effects of these beam parameters on the angular distribution of DR and provide solutions to this difficulty. These include use of the horizontal and vertical polarization components of the radiation from a single slit and interferences from two inclined slits. Examples of DR diagnostics for a 500 MeV beam are presented and the current limitations of the technique are discussed.

R. B. Fiorito
Catholic University of America, Washington, DC 20064
email : rfiorito@rocketmail.com

D. W. Rule
Carderock Division, Naval Surface Warfare Center, W. Bethesda, MD 20817

1 Introduction

The new generation very high power radiation devices such as short wavelength free electron lasers and single pass spontaneous emission (SASE) devices for the generation of intense uv and x-ray beams requires the development of linear accelerators which produce optical quality charged particle beams. The high power, small size and low emittance of these beams present an enormous challenge for both the diagnostic measurement of beam parameters and the accurate positioning and control of these beams. Conventional screens or other interceptive probes are incompatible with the operation of such accelerators in many instances. Non interceptive devices such as wall monitor arrays, give limited beam information. Other types of monitors, such as synchrotron monitors, while non-invasive, cannot be used in linear beam line geometries. Hence the development of low cost, compact, nondestructive monitors capable of measuring multiple beam parameters would be very useful for many high power beam applications.

We have investigated how the properties of diffraction radiation (DR) can be used to measure beam divergence, energy, position, transverse beam size and emittance. DR devices such as slits or circular apertures through which the beam passes offer minimal perturbation to the beam, respond rapidly to changes in beam parameters and are inherently compact, so that they can be implemented at many places in the beam line.

Diffraction radiation (DR) is produced when a charged particle passes through an aperture or near an edge or interface between media with different dielectric properties. DR is closely related to transition radiation (TR), which is produced when a charged particle traverses the boundary between media with different dielectric constants. DR has been studied theoretically since the early 1960's, [1-5]. However, in contrast to TR, which has been well investigated experimentally and is now used extensively for beam diagnosis, we are aware of only two experimental studies of DR in the literature [6],[7]. In only one of these investigations [6] was DR actually used as a beam parameter diagnostic, i.e. to measure the beam bunch length. Furthermore, in this study forward and 180° backward directed DR and TR were observed simultaneously. This situation complicated the comparison of measured to theoretically predicted DR properties. Therefore, to avoid such difficulties and for experimental convenience, it is advantageous to observe the radiation from an inclined aperture, e.g. a slit inclined at 45° , which produces DR both in the forward direction and in the direction of specular reflection of the virtual photons associated with the particle, i.e. at 90 degrees with respect to the beam velocity.

The detailed nature of the far field angular distribution (AD) of *forward* directed DR has been derived and discussed by Ter-Mikaelian [4] for an electron normally incident on a circular aperture and a slit in an infinite, thin plane. The fields and AD of DR from an electron incident on a single edge (half plane) inclined at an arbitrary angle with respect to the velocity vector of the particle have also been derived and discussed in Refs. [2], [4] and [8]. Although some authors have surmised that reflected DR from an inclined circular aperture or slit has properties similar to reflected TR [9-10], a derivation, from first principles, of the spectral-angular distribution of reflected DR from such apertures has not been previously

available in the literature. We present here solutions for the fields and the horizontally and vertically polarized intensities of DR from an inclined slit for two orientations of the slit edge, i.e. parallel and perpendicular with respect to the plane of incidence.

Previous theoretical investigations of forward directed DR generated from electron beams passing through circular apertures and slits [9-12] have examined the potential use of the far field angular distribution (AD) to diagnose beam properties such as position with respect to the center of the aperture, beam size, trajectory angle, divergence and energy. The potential advantage and difficulty in using the AD of DR for beam diagnostics is that it depends on the beam position (size) as well as the beam divergence and energy. In contrast, the AD of TR depends only on the beam divergence and energy. The challenge for the application of the AD of DR as a diagnostic then is to devise a means to separate out the competing effects of divergence and beam size on this observable.

We have developed a number of ways to address and solve this problem. We demonstrate here how the measurements of the horizontal and vertical polarization components of backward reflected DR from a single slit can be used to separate out the effects of beam size perpendicular to the slit edge and the component of divergence parallel to the slit edge. Furthermore, we show how the measured AD's for two different orthogonal orientations of the slit axis, can be used to determine the components of beam size and divergence in two orthogonal directions, i.e. the directions perpendicular and parallel to the plane of incidence. In addition we suggest how the interferences from two slits can be used to make a sensitive measurement of divergence alone.

2 Diffraction Radiation Properties

When a charged particle or ensemble of particles passes through an aperture or near an edge at a distance d , appreciable DR is generated when the condition: $d \lesssim \gamma \bar{\lambda}$ is fulfilled, where $\bar{\lambda} = \lambda/2\pi$, and λ is the observed wavelength. Table I. presents typical wavelengths of DR observed from a slit whose width $a = 2d = 2mm$ for a variety of lepton and hadron beams. Table I. shows, for example, that DR is produced in the optical part of the spectrum (i.e. IR to visible) for electrons with energies in the range of 0.5 - 5 GeV.

Table I.
Typical wavelengths of diffraction radiation generated from a 2-mm wide slit for various accelerators

E(GeV)	γ	$\lambda(\mu m)$	Accelerator
0.5	10^3	6.30	APS
5.0	10^4	0.630	CEBA
50.0	10^5	0.063	SLAC
250.0	250	25.00	RHIC
10^3	10^3	6.30	FNAL

When the observed DR wavelength is much smaller than the transverse or longitudinal size of a charged particle bunch, incoherent DR is produced independently from each particle and the total intensity $I \sim N$, the number of particles in the bunch. For wavelengths comparable to the bunch dimensions coherent DR is observed with an intensity $I \sim N^2$. The DR diagnostic methods we will present can utilize either incoherent or coherent DR. However, for simplicity and to illustrate and emphasize the basic methodology we will concern ourselves here only with the analysis of incoherent DR. Furthermore, since we have discussed DR diagnostics using circular apertures elsewhere [10], we will focus our attention in this paper to the generation of DR from slits. An extended analysis of coherent DR from a slit will be presented in a future work.

3 Theory of Backward Diffraction Radiation from an Inclined Slit

3.1 Parallel orientation of slit with respect to the plane of incidence

A relativistic charged particle passing through a slit in a conducting screen emits diffraction radiation in the forward and backward directions, the latter in the direction of specular reflection of the virtual photons associated with the relativistic particle. The peak intensity of diffraction radiation, like transition radiation, occurs at an angle $\theta \sim \gamma^{-1}$, where θ is measured from the direction of the particle's velocity vector \mathbf{v} for forward DR, and from the direction of specular reflection for backward DR.

Figure 1A. shows a side view, and Figure 1B. a top view, of the cone of backward diffraction radiation emitted by a charge passing through a slit which is inclined at the angle Ψ with respect to the velocity vector and oriented such that its edge is horizontal or parallel to the plane of incidence (\mathbf{n}, \mathbf{v} plane), where \mathbf{n} is the unit vector normal to the plane of the slit, i.e. the (x', y') plane. Additionally, the particle passes through the slit with an offset δ in the vertical (y') direction measured from the center of the slit which is defined by the x' axis. For simplicity, we have not drawn the forward directed cone of DR which is also generated in the direction \mathbf{v} . Figures 1A. and 1B. show the coordinate system (x, y, z) used to describe the radiation fields associated with the wave vector \mathbf{k} observed in the backward direction (i.e. directed along the z axis). The slit is assumed to be an infinitely thin conducting screen with infinite extent in the x' and y' directions beyond the slit aperture.

Our calculation of the backward reflected DR fields employs three different concepts (a) the Huygens-Fresnel diffraction approach, following the treatment given by Ter-Mikaelian [4] for the case of forward DR, (b) the concept of backward reflected pseudo photons, used by Wartski [13] to calculate reflected transition radiation and (c) a form of Babinet's principle. Our approach is quite different and mathematically much less complex than the exact Wiener Hopf method used by previous researchers to calculate backward DR from a single edge [2,4]. In addition, our method is generally applicable to other geometries where the Wiener Hopf technique is very difficult to implement.

Consider a thin reflecting metal screen S_∞ with infinite extent. A charged particle crossing this surface produces the well known forward and backward transition radiation. Compare this to the case of Fig. 1., where the slit has an area S_1 and the conducting screen has an area S_2 . Babinet's principle states that the transition radiation (TR) field from the infinite conducting screen, S_∞ , can be obtained from a Huygen's Fresnel integral over the infinite area $S_\infty = S_1 + S_2$, so that the TR field can be expressed as $\vec{E}_\infty = \vec{E}_1 + \vec{E}_2$ where \vec{E}_1 and \vec{E}_2 are those parts of the field which are obtained from a Huygen's Fresnel integral over the areas S_1 and S_2 , respectively [8]. If material of area S_1 is removed, then the field $\vec{E}_2 = \vec{E}_\infty - \vec{E}_1$, where \vec{E}_2 is the desired backward DR field. Note that if the area $S_1 \rightarrow 0$, $\vec{E}_2 \rightarrow \vec{E}_\infty$, and the DR field approaches that of TR.

The incident field in the Huygens-Fresnel integral is the field associated with the relativistic particle, \vec{E}_i . Using Ter-Mikaelian's approach to calculate the diffraction radiation field and Wartski's method of calculating backward reflected radiation, we can express the x and y components of the radiation field as

$$E_{x,y}(k_x, k_y) = r_{\parallel,\perp}(\omega, \Psi) \frac{1}{4\pi^2} \iint E_{ix,iy}(x, y) e^{-i\vec{k}\cdot\vec{\rho}} dx dy \quad (1)$$

where $E_{ix,iy}$ are the components of the field of the incoming charged particle and k_x and k_y are the components of the wave vector \mathbf{k} in the plane normal to the direction \mathbf{z} shown in Figure 1A. and 1B. As is the case for TR, there are generally three components to the radiation: direct, reflected and transmitted. However, for an opaque, highly conducting screen, the dominant term for backward TR or DR production is the reflected component. The fields E_x and E_y for backward TR and DR are thus proportional to the Fresnel reflection coefficients r_\parallel and r_\perp , respectively. In Eq. (1), the integral over the area S_2 is done in terms of the coordinates (x, y) of Figures 1 and 2. The far field reflected spectral intensity of DR is found by integrating the flux of pseudo photons reflected off the surface S_2 , which pass through the plane that is perpendicular to the direction \mathbf{z} , i.e. the direction of specular reflection of incident pseudo photons having a wave vector \mathbf{k} , which is parallel or closely parallel to the velocity vector \mathbf{v} . The phase term in Eq. (1), which is a function of $\vec{\rho} = (x', y')$, a vector lying in the plane of the screen, can be related to the coordinates (x, y) by the transformations $x = x' \sin(\Psi)$, $y = y'$, and the differential elements of area by $dx dy = dx' dy' \sin(\Psi)$. The detailed solution of the integral in Eq. (1) is presented in the Appendix.

The results are:

$$E_x(k_x, k_y) = \frac{ier_\parallel(\omega, \Psi) \bar{k}_x}{4\pi^2 v} \left[\frac{1}{(f - ik_y)} e^{-a_1(f - ik_y)} + \frac{1}{(f + ik_y)} e^{-a_2(f + ik_y)} \right], \quad (2)$$

which is identical to Eq. (31.18) of Ref. [4], except for the reflection coefficient $r_\parallel(\omega, \Psi)$, and the scalar quantity $\bar{k}_x \equiv k_x - [k/(2\gamma^2)] \cot \Psi$, and

$$E_y(k_x, k_y) = \frac{er_\perp(\omega, \Psi)}{4\pi^2 v} \left[\frac{1}{(f - ik_y)} e^{-a_1(f - ik_y)} - \frac{1}{(f + ik_y)} e^{-a_2(f + ik_y)} \right], \quad (3)$$

which is identical to Eq. (31.19) of Ref. [4], except for the factor $r_{\perp}(\omega, \Psi)$. Here $a_{1,2} = a/2 \pm \delta$, $f = [\bar{k}_x^2 + \omega^2 / (v^2 \gamma^2)]^{1/2}$, $v = |\mathbf{v}|$, $k_x = k \sin \theta_x$, $k_y = k \sin \theta_y$ and $\theta_{x,y}$ are the projected angles of the vector \mathbf{k} into the x, z and y, z planes, respectively.

The horizontally polarized intensity (i.e. parallel to the slit edge) and vertically polarized intensity (i.e. perpendicular to the slit edge), which are observed in the plane perpendicular to the direction of specular reflection, are defined in terms of the x and y components of the fields:

$$\begin{aligned} \frac{d^2 N_{horiz.}}{d\omega d\Omega} &= \frac{2\pi^2 k^2 c}{\hbar\omega} |E_x|^2 \\ &= |r_{\parallel}|^2 \frac{\alpha k^2 \bar{k}_x^2 e^{-af}}{4\pi^2 \omega f^2 (f^2 + k_y^2)} [\cosh(2f\delta) + \sin(ak_y + \Phi(k_x, k_y))] \end{aligned} \quad (4)$$

and

$$\begin{aligned} \frac{d^2 N_{vert.}}{d\omega d\Omega} &= \frac{2\pi^2 k^2 c}{\hbar\omega} |E_y|^2 \\ &= |r_{\perp}|^2 \frac{\alpha k^2 e^{-af}}{4\pi^2 \omega (f^2 + k_y^2)} [\cosh(2f\delta) - \sin(ak_y + \Phi(k_x, k_y))] \end{aligned} \quad (5)$$

respectively, where

$$\Phi(k_x, k_y) = \sin^{-1}[(f^2 - k_y^2)/(f^2 + k_y^2)] = \cos^{-1}[-2fk_y/(f^2 + k_y^2)], \quad (6)$$

and $\alpha \simeq \frac{1}{137}$ is the fine structure constant.

The equations for vertically polarized *forward* diffraction radiation intensity, first obtained by Ter-Mikaelian [4] and later rewritten and presented in Ref. [9], are both equivalent to Eq. (5) without the factor $|r_{\perp}|^2$. Note, however, that the equations for phase term, $\Phi(k_x, k_y)$ presented in Ref. [9] are incorrect. The correct relationships are given in Eq. (6).

3.1.1 Limiting Forms for Backward DR at 45°

Under the usual small angle approximation for observation of TR and DR from relativistic particles, i.e. $v \approx c$, $\theta \sim \gamma^{-1} \ll 1$, the quantities $\bar{k}_x \approx k_x \approx k\theta_x$, $k_y \approx k\theta_y$, and $k_z \approx k$. We then can consider several limiting forms for backward DR.

(1) *Single Edge Limit*: When either a_1 or $a_2 \rightarrow \infty$, the sinusoidal term in Eqs. (4) and (5), which represents the interference between the intensities from each edge of the slit, disappears and expressions for the horizontal and vertical intensities of DR from a single edge are obtained. The addition of the horizontal and vertical intensities taken in this limit produces an expression for the total DR intensity which is identical to that obtained using the exact Wiener Hopf approach (see Ref. [8], Eq. (14)). The correspondence of the results of our calculations to those calculated using exact theory is a strong confirmation of the validity of our method for calculating backward reflected DR.

(2) *Small Displacement Limit*: When δ , the particle displacement from the center of the slit, is small, i.e. $\delta \ll \gamma\bar{\lambda} \sim a$, the hyperbolic cosine in Eqs. (4) and (5) can be expanded in a Taylor series. Retaining terms only up to second order, and using the small angle approximations given above, Eqs. (4) and (5) become:

$$\begin{aligned} \frac{d^2 N_{horiz.}}{d\omega d\Omega} &= |r_{\parallel}|^2 \frac{\alpha}{4\pi^2\omega} \gamma^2 \frac{X^2}{(1+X^2)} \frac{e^{-R(1+X^2)^{1/2}}}{(1+X^2+Y^2)} \\ &\cdot [1 + 2\left(\frac{\delta}{\gamma\bar{\lambda}}\right)^2(1+X^2) + \sin(RY + \Phi'(X, Y))] \end{aligned} \quad (7)$$

and

$$\begin{aligned} \frac{d^2 N_{vert.}}{d\omega d\Omega} &= |r_{\perp}|^2 \frac{\alpha}{4\pi^2\omega} \gamma^2 \frac{e^{-R(1+X^2)^{1/2}}}{(1+X^2+Y^2)} \\ &\cdot [1 + 2\left(\frac{\delta}{\gamma\bar{\lambda}}\right)^2(1+X^2) - \sin(RY + \Phi'(X, Y))] \end{aligned} \quad (8)$$

where we have introduced the new variables $X = \gamma\theta_x$ and $Y = \gamma\theta_y$, the x and y projected angles scaled in units of γ^{-1} , $R \equiv a/\gamma\bar{\lambda}$ and the reduced phase term

$$\Phi'(X, Y) = \sin^{-1}[(1+X^2-Y^2)/(1+X^2+Y^2)] = \cos^{-1}[-2(1+X^2)^{1/2}Y/(1+X^2+Y^2)]. \quad (9)$$

(3) *TR Limit*: Additionally, when $R \ll 1$ and $\delta \ll \gamma\bar{\lambda}$, Eqs. (7) and (8) each reduce to one half the intensity of TR, which is the expected correct limit. In this regime the particle radiates as if the slit in the screen were absent.

3.2 Perpendicular orientation of the slit with respect to the plane of incidence

Figures 2A. and 2B. illustrate the case in which the slit is oriented such that the edge is perpendicular to the plane of incidence, i.e. the plane containing \mathbf{v} and \mathbf{n} the normal to the plane of the screen. In this case, the offset ε of the particle velocity vector from the center of the slit is in the direction Y' and the radiation fields E_x and E_y can be shown to be the same as those given above in Eqs. (2) and (3) but with $a_1 \rightarrow a_1 \sin \Psi$, $a_2 \rightarrow a_2 \sin \Psi$ and $\delta \rightarrow \varepsilon \sin \Psi$. Also, $E_x \propto r_{\perp}(\omega, \Psi)$ and $E_y \propto r_{\parallel}(\omega, \Psi)$ since, for this orientation of the slit, \vec{E}_x is perpendicular and \vec{E}_y is parallel, respectively, to the plane of incidence. Then E_x and E_y take the same forms as Eqs. (2) and (3), with the coefficients r_{\perp} and r_{\parallel} interchanged. Similarly the vertical and horizontal intensity components take on the same forms as Eqs. (4) and (5), with the coefficients $|r_{\perp}|^2$ and $|r_{\parallel}|^2$ interchanged.

In Ref. [8] it has been shown that an exact calculation of reflected DR produced by a particle traveling with a velocity with a parallel component along the direction of the edge of a semi-infinite screen [2] reduces, in the limit $\gamma \gg 1$, to the same result as that of a particle whose velocity vector is purely perpendicular to the edge (see Eqs.(7) and (14) of

Ref.[8]). The former situation corresponds to the geometry of Figure 1. as discussed above in Section 3.1; the latter situation corresponds to the geometry of Figure 2., which is discussed in this Section. As in the parallel case, the single edge results for the geometry of Fig. 2. are completely reproduced using our approach in the limit a_1 or $a_2 \rightarrow \infty$. Furthermore, in the perpendicular incidence case the small angle, relativistic limit produces the same forms for the horizontal and vertical intensities as the parallel incidence case, i.e. Eqs. (7) and (8), but with the coefficients $|r_{\perp}|^2$ and $|r_{\parallel}|^2$ interchanged. In addition, when $R \ll 1$, the horizontal and vertical intensities each go to the same TR limit as in the parallel incidence case. These results provide further evidence of the soundness of our theoretical approach.

For the sake of simplicity and to illustrate the main results of our analysis of DR from slits, we will present numerical examples only for the case of the slit oriented with its edge *parallel* to the plane of incidence . However, numerical results can easily be obtained for the perpendicular orientation by simple substitution of variables as listed above.

4 Discussion and Computational Results

4.1 General properties of DR

Eqs. (5) and (6) indicate that the highest yield of backward DR observed in the IR to visible part of the spectrum will be generated when the surface of the slit is a highly conducting mirrored surface. In the case $|r_{\perp}|^2 \simeq |r_{\parallel}|^2 \simeq 1$. and for $\gamma \gg 1$, Eqs. (7) and (8) show that the polarization components are the same as forward DR. These equations also reveal some interesting characteristics of DR from a slit, which have not been fully discussed in previous studies, and which can be easily visualized with the help of three dimensional plots of intensity observed in the X, Y plane.

Figs. 3A. and 3B. show the horizontal and vertical components, respectively, of the intensity of DR for a value of the ratio $R = a/(\gamma\bar{\lambda}) = 0.5$. Similarly, Figs. 4A. and 4B. show the component intensities for $R = 2.0$. The intensity axis (Z) in these Figures is scaled in proportion to the corresponding intensity component of transition radiation. For example, Fig. 3A indicates that the peak intensities of horizontal and vertical DR, respectively, are about 25% and 80% that of TR , when $R = 0.5$. Figures 3. and 4. also show that diffraction fringes are present in both polarization components, but are only observed in the Y direction (perpendicular to the slit edge) for both the orientations shown in Figs. 1 and 2. This can be deduced directly by an examination of the term $\sin(RY + \Phi'(X, Y))$ in Eqs. (7) and (8), i.e. the frequency of oscillation is determined solely by the value of k_y component of the wave vector represented through the variable R . Secondly, the interferences in the horizontal and vertical intensities are 180° out of phase. This is evident by the presence of the difference in the sign of the sinusoidal terms in each component. Thus, in general, the maxima of the vertical component along the Y axis occur at the minima of the horizontal component.

One further observes that the equation for horizontal intensity, Eq.(7) contains the factor $X^2/(1 + X^2)$, which is not present in Eq.(8) for the vertical intensity. This term, which

is similar to the form of TR, forces the horizontal component to have a null at $X = 0$ for every value of Y . A comparison of the ratio of vertical to horizontal intensities reveals that the vertical component is larger than the horizontal component, and that ratio becomes smaller as R decreases approaching unity as $R \rightarrow 0$, i.e. the transition radiation limit. Also, as R becomes large the DR intensity drops off exponentially. Thus the value of R should be kept to a minimum to maximize the observed intensity of DR. We have chosen the values $R = 0.5$ and 2.0 to show that measurable horizontal and vertical intensity levels can be achieved for reasonable experimental conditions and to demonstrate that the ratio of vertical to horizontal intensity depends on the value of R . For example, a value of $R = 2$ applies to the case when the beam energy $E_b = 500 \text{ MeV}$, the slit width $a = 2 \text{ mm}$ and the wavelength $\lambda \simeq 3 \mu\text{m}$. By change of the parameters a and λ , or by use of different values of R , other workable combinations are possible for a given beam energy. Note that as the beam energy increases, a smaller value of R can be achieved for the same wavelength and slit size. Since the intensity of DR, like TR, is proportional to γ^2 (see Eqs. (7) and (8)), DR becomes progressively more intense as hence easier to detect as the beam energy increases.

In general, the sum of horizontal and vertical polarization intensity components will be observed by a detector in the X, Y plane. Thus, if the angular distribution of DR is imaged, e.g. by using a camera with a lens focussed at infinity, the sum of horizontal and vertical distributions will be superimposed. However, either distribution can be imaged separately by placing a rotatable polarizer in front of the lens. We will show that each of these intensity components provides information about the beam size and divergence in each of two orthogonal directions and, furthermore, that all of these beam parameters can be measured by proper analysis of the horizontally and vertically polarized intensities.

4.2 Effect of Beam Parameters on the Angular Distribution of DR

4.2.1 Beam Size

The above discussion shows that both the horizontal and vertical DR spectral-angular distributions are functions of the beam position δ relative to the center of the slit. This effect has been previously considered [9,11] as a possible diagnostic of the beam position and size. In Ref. [9] it was shown that the effects of beam size and offset on the angular distribution of DR are the same. Also, in Ref. [11] it was shown that the DR intensity is a minimum for a beam centered in the slit, i.e. zero offset. Since the beam can be centered by monitoring and steering the beam to minimize the total intensity, the offset can be nullified or otherwise determined, for example, by use of a standard wall current monitor. The remaining effects on the angular distribution of the DR will then be the beam size in the direction perpendicular to the slit edge and the two orthogonal components of the beam divergence.

To determine the effect of beam size on the intensity components, we assume that the beam centroid has been centered in the slit by means of one of the previous methods described above and that any particle within the finite beam spatial distribution has the same effect as the offset of a single particle. We further assume that the beam has a separable spatial distribution given by $S = S_1(\delta) \cdot S_2(\varepsilon)$, where δ and ε are in the directions y' and x' ,

respectively. For the parallel orientation of the slit, δ and ε are perpendicular and parallel, respectively, to the slit edge. Integration of the distribution S over δ and ε produces the average beam sizes $\langle\delta\rangle$ and $\langle\varepsilon\rangle$. Because of the simple dependence of the above expressions for horizontal and vertical intensity on the variable δ , an integration of S over the intensity components is mathematically equivalent to a simple replacement the variable δ with its average value $\langle\delta\rangle$. To simplify the notation in the remainder of the text we will identify and refer to δ and ε as the orthogonal rms beam size components, which are perpendicular and parallel, respectively, to the plane of incidence.

4.2.2 Beam Divergence

Ref. [9] has examined the effect of beam size perpendicular to the edge of a slit on the vertical intensity component of forward DR in the absence of divergence. A discussion of the effect of beam size on the horizontal component was dismissed because of its much lower intensity in comparison to the vertical intensity - an effect which was due to the rather large value of $R = 2\pi$ used in the analysis. However, for any realistic beam, the divergence is not negligible and affects both the horizontal and vertical intensities of DR. Furthermore, in general, the horizontal component of DR is not negligible in comparison to the vertical component and, as we will show, this component provides important information on the component of beam divergence parallel to the slit edge. It is therefore important to analyze both the effect of beam size and divergence on the vertical and horizontal intensity components to fully assess the diagnostic potential of DR.

The effect of divergence must be taken into account by performing a two dimensional convolution of a distribution of particle trajectory angles projected in the X, Z and Y, Z planes (e.g. separable Gaussian distributions in θ_x and θ_y). However, we have shown by numerical calculation that the effect of the rms divergence δ' on the *horizontal* component of the DR intensity, and the effect of the rms divergence ε' on the *vertical* component is insignificant for $\delta', \varepsilon' \lesssim 0.2$, a value which is large by the standards of most high quality accelerators. Then, to a good approximation, a one dimensional convolution of a line scan of the horizontal or vertical intensity calculated either in the plane defined by $Y = const.$ or $X = const.$ can in principal be used to predict the effects of the beam divergences ε' and δ' , respectively. Inversely, these divergences can be determined by fitting the convolved intensities to measured data.

Horizontal Intensity Component The effect of the divergence ε' , the component parallel to the incidence plane, on the horizontal intensity component can be estimated by neglecting the beam size term. Consider the term X^2 in the numerator of the horizontal component Eq.(7). Because of the presence of this term, a convolution of the horizontal intensity component with a distribution of particle angles $G(X, \varepsilon')$ will have the maximum effect on this component. Furthermore, the effect of ε' will be maximized near the center of the pattern where the horizontal intensity goes to zero in the absence of divergence. One can estimate this effect by setting the variable Y in Eq. (7) equal to a constant value

$Y = \delta' = \text{const.}$, and noting the effect on a line scan of the one dimensional convolution of the horizontal intensity with e.g. the Gaussian distribution: $G(X, \varepsilon') = \frac{1}{\sqrt{2\pi\varepsilon'^2}} \exp(\frac{-X^2}{2\varepsilon'^2})$.

Figure 5. shows two such normalized scans of a 1D convolution of horizontal intensity (Eq. (7)) with G for two different values of the variable, $Y = \delta' = 0.2$ and $Y = 0$. In this calculation, $R = 2.0$ and $\varepsilon' = 0.1$. As Fig. 5. shows, there is no discernible difference between the two patterns. Then only a small error will be made by setting the variable Y equal to a constant and performing a one dimensional convolution over X to infer the effect of the divergence ε' . Inversely, it is possible to measure the divergence, ε' from line scans of horizontally polarized DR for a number of Y values by comparing the measured intensity scans to theoretically convolved line scans in the variable X , which are parameterized by the variable ε' .

Now consider the effect of the beam size δ measured perpendicular the plane of incidence, which is also perpendicular to the slit edge for the orientation shown in Fig. 1., on the horizontal intensity. Note that the effect of beam size ε or any displacement parallel to the slit edge has no effect on this component. To compare the effect of the beam size δ with effect of the divergence ε' , consider a line scan of the horizontal intensity component observed over a finite bandwidth ($\Delta\omega$) taken in the plane, $Y = 0$. Eq. (7) then reduces to:

$$\frac{dN_{Horiz.}}{d\Omega} = |r_{\parallel}|^2 \frac{\alpha\gamma^2 \Delta\omega}{2\pi^2 \omega} \frac{X^2}{(1+X^2)^2} e^{-R(1+X^2)^{1/2}} \cdot [1 + (\frac{\delta}{\gamma\lambda})^2(1+X^2)]. \quad (10)$$

A convolution of this expression with the Gaussian distribution, $G(X, \varepsilon')$, evaluated at $X = 0$, to first order in ε'^2 , gives

$$\frac{dN_{Horiz.}}{d\Omega} \otimes G(X, \varepsilon') \propto \varepsilon'^2 [1 + (\frac{\delta}{\gamma\lambda})^2]. \quad (11)$$

Thus, while it is still present, the effect of the beam size δ on the horizontal component will be much smaller than that of the divergence ε' . Figure 6. shows how a change in the divergence ε' affects the horizontal intensity for a fixed value of the beam size $\delta = 300\mu$. As predicted from Eq.(11), the effect of ε' is maximum near the origin. Conversely, the shape of pattern shape in the vicinity of the origin can be used to separate out and measure the divergence ε' .

Figure 7. shows the effect of the beam size, δ on a line scan of the horizontal intensity (Eq. (12)) taken in the X, Z plane, i.e. $Y = 0$, when $\varepsilon' = 0$ and $R = 2$. Figure 7. shows that a change in δ has no effect on the horizontal component in the region near $X = 0$, but does affect the peak value of the intensity observed at $|X| \approx 1$ and the fall off of intensity for $|X| > 1$, for $\delta > 50\mu$. Numerical calculations indicate similar variation of the intensities with beam size and divergence for $R = 0.5$. Therefore, for simplicity, we will only present below numerical results for a single value of the parameter $R = 2$.

Vertical Intensity Component A procedure similar to the one described above can be used to show that the effect of the divergence ε' has a minimal effect on the vertical intensity

distribution. Figure 8. shows two scans of the vertical intensity observed in Figure 4B in the planes $X = \varepsilon' = 0.2$ and $X = 0$. As similarly shown in Fig. 5., the difference in the two scans is very small. Thus, it should be possible to use a one dimensional convolution to infer the effect of the divergence δ' , on line scans of vertically polarized DR (measured in the Y direction) for a number of X values.

By comparing the measured intensity scans to a set of one dimensional convolutions in Y parameterized by the divergence component δ' , one would hope to be able to measure this quantity. However, for the vertical intensity component the effect of the beam size δ is comparable to that of the divergence δ' . To see this consider an observation of the vertical intensity component (Eq. (8)) in the Y, Z plane i.e. $X = 0$. For a finite bandwidth ($\Delta\omega$) measurement, Eq. (8) produces the vertical angular distribution

$$\begin{aligned} \frac{dN_{Vert.}}{d\Omega} = & |r_{\perp}|^2 \frac{\alpha}{4\pi^2} \frac{\Delta\omega}{\omega} \gamma^2 \frac{e^{-R}}{(1+Y^2)} \\ & \cdot \left[1 + 2\left(\frac{\delta}{\gamma\lambda}\right)^2 + \frac{2Y \sin(RY) - (1-Y^2) \cos(RY)}{(1+Y^2)} \right]. \end{aligned} \quad (12)$$

To compute the effect of the divergence δ' one must take the convolution of Eq. (12) with a distribution over the variable Y , e.g. the Gaussian distribution. $G(Y, \delta') = \frac{1}{\sqrt{2\pi\delta'^2}} \exp(-\frac{Y^2}{2\delta'^2})$. We have performed this computation numerically to see how the effects of beam size and divergence compare. Figure 9. shows a vertical intensity scan taken at $X = 0$, for a fixed value of the beam size $\delta = 200\mu$ and $R = 2.0$ for several values of divergence δ' . Figure 10. shows the effect of a change in the beam size, δ on similar scans for the divergence value $\delta' = 0$. A comparison of Figs. 9. and 10. clearly indicates that the effect of divergences $\delta' < 0.2$ will compete significantly with the effect of beam sizes $\delta \lesssim 300\mu$ on the angular distribution of the vertical intensity component. Thus, in general, neither effect can be neglected and the two effects are not separable for this component.

4.3 Strategies for separating beam size and divergence effects

4.3.1 Use of slit oriented perpendicular to the plane of incidence

In order to help separate out the competing effects of beam size and divergence, we have considered two alternative strategies. One method is to rotate the slit (or insert another into the beam line) so that the slit edge is perpendicular to the plane of incidence (see Fig. 2A.). In this configuration the horizontal intensity component of the DR, convolved with the Gaussian function, $G(X, \delta') = \frac{1}{\sqrt{2\pi\delta'^2}} \exp(-\frac{X^2}{2\delta'^2})$, can be used to measure the divergence δ' , which is now the component of divergence measured parallel to the slit edge. For this orientation the horizontal component is highly sensitive to δ' and only weakly depend on the beam size ε , which is now the component of the beam size perpendicular to the slit edge. Evaluating the convolved horizontal intensity at $X = 0$, we obtain

$$\frac{dN_{Horiz.}}{d\Omega} \otimes G(X, \delta') \propto \delta'^2 \left[1 + \left(\frac{\varepsilon}{\gamma\lambda}\right)^2 \right]. \quad (13)$$

Eq.(13) is the direct analog of Eq.(11) above which, as shown in the previous section, can be used to determine ε' . For the perpendicular orientation of the slit edge, however, the center of the horizontal AD pattern is sensitive to, and can be used to measure, the divergence component δ' .

The vertical DR intensity component for this orientation of the slit is:

$$\begin{aligned} \frac{dN_{Vert.}}{d\Omega} = & |r_{\parallel}|^2 \frac{\alpha}{4\pi^2} \frac{\Delta\omega}{\omega} \gamma^2 \frac{e^{-R}}{(1+Y^2)} \\ & \cdot [1 + 2(\frac{\varepsilon}{\gamma\lambda})^2 + \frac{2Y \sin(RY) - (1-Y^2) \cos(RY)}{(1+Y^2)}], \end{aligned} \quad (14)$$

which is the direct analog of Eq. (12). A one dimensional convolution of Eq. (14) with the Gaussian distribution $G(Y, \varepsilon') = \frac{1}{\sqrt{2\pi\varepsilon'^2}} \exp(\frac{-Y^2}{2\varepsilon'^2})$, produces a pattern that is sensitive to the divergence ε' as well as the beam size ε . Thus for the perpendicular slit orientation the divergence ε' and beam size ε have comparable effects and it is not possible to distinguish between them using the vertical intensity component alone.

4.3.2 DR Interferometry

The second strategy we have devised to separate out and measure divergence is to use the interference of DR produced from two slits inclined at 45° with respect to the beam velocity in a configuration which is the direct DR analogy to a Wartski OTR interferometer[13]. In such a system forward DR from the first slit reflects from the second slit surface and interferes with backward DR generated from the second slit. The interferences produced by the two intensities will be superimposed on the single slit DR intensity. Figure 11. shows one possible configuration for a DR interferometer composed of two slits oriented with their edges parallel to the plane of incidence. The equation for interference DR, in analogy to TR, is obtained by multiplying Eqs. (7) and (8) by an additional interference term which is due to the difference in phase between forward and backward DR. The expressions for the horizontal and vertical intensity components are of the form:

$$\frac{dN_{Horiz,Vert}^{(I)}}{d\Omega} = 4 \frac{dN_{Horiz,Vert}^{(S)}}{d\Omega} \sin^2\left(\frac{L}{2L_V}\right) \quad (15)$$

where the superscript I refers to the two slit (interferometer), and S to the single slit angular intensity distributions, respectively, $L_V \equiv \lambda/\pi(\gamma^{-2} + \theta^2)$ is the coherence length in vacuum for TR and DR, which represents the distance over which the particle's field and the TR or DR photon differ in phase by one radian and L is the path length between the slits.

For a fixed wavelength and energy the single slit term varies slowly with the angle θ . Then a convolution of Eq.(15) with a distribution of beam angles will chiefly effect the interference term $\sin^2(\frac{L}{2L_V})$. The interference fringe visibility is then a function of the angular divergence and is independent of beam size effects. Thus it should be possible to use DR interferences to obtain a measurement of the beam divergence alone. Also as is the case with interference

OTR, measurements of the two polarized components of interference DR can be used to measure orthogonal components of the beam divergence[14]. The interference fringes, which are superimposed on the single slit angular distribution, provide increased sensitivity to angular differences in the particle trajectory angles and therefore smaller values of divergence ($\delta', \varepsilon' \lesssim 0.05$) can be measured with an interferometer than with a single slit alone.

Figures 12. and 13. show the vertical and horizontal components of intensity, respectively, from a DR interferometer produced by an electron beam with energy $E = 500$ MeV, $R = 2$, $\lambda = 3.2\mu\text{m}$, $\delta = 200\mu$ and $\delta' = 0.05$. The separation distance $L = 6L_V = 3$ meters for this beam energy. In any DR interferometer the angular distribution of the forward DR from the first foil will be partially cut off by the presence of the second slit in such a configuration. If the path length between the slits is large, the total angular field will only be cut off in the center of the pattern by a small amount. Thus only a small fraction of the interference patterns ($1/6\gamma$ for the parameter range specified above) will be cut out. This effect is not shown in Figs. 12. and 13.

In contrast to the very weak effect of a small value of divergence, i.e. $\delta' = 0.05$, on single slit DR (see Figs. 7. and 9.), the effect of this divergence on the DR interference fringe visibility is clearly visible. Since the fringes are well modulated out to $Y \sim 4$, the cutoff of the field of view due to the second aperture will have a negligible effect on a measurement of the divergence, which uses the interference pattern. With the help of a second camera or imager, a simultaneous measurement of backward DR from the first slit can be made and thereby provide addition single slit data for extracting the beam size.

At the present time the use of the angular distribution of DR for diagnostics is practically limited to beams with moderate to high energies by the vacuum coherence length $L_V \sim \gamma^2\lambda$. The DR produced by upstream sources such as beam line discontinuities or other apertures will destructively interfere with backward DR generated from a diagnostic aperture when the distance between the upstream source and the aperture is much less than L_V . Also, the successful application of interference DR to measure beam divergences $\delta', \varepsilon' \lesssim 0.05$ requires that the inter-aperture distance $L \gtrsim 5L_V$. Therefore, the diagnostic techniques described in this paper are limited to observation wavelengths and beam energies which do not give rise to an impracticably long coherence length for the accelerator facility being used. The means to overcome this limit must be developed before the methods described here can be applied to beams with very high energy.

5 Summary

We have developed a new method to calculate backward reflected diffraction radiation from any type of aperture. Using this method we have derived the equations for backward horizontal and vertically polarized spectral-angular intensities of DR from a slit inclined at an arbitrary angle with respect to the particle velocity. We have obtained results for two orthogonal orientations of the slit edges, i.e. parallel and perpendicular to the plane of incidence. The results of our calculations reduce in the single edge limit precisely to those previously

derived using the exact Wiener Hopf method. However, in contrast to the Wiener Hopf approach, which has been successfully used to calculate DR from one type of aperture only, i.e. the single edge, our approach is readily applicable to any type of aperture and is much simpler to employ.

From an analysis of backward DR for the two orientations of the slit mentioned above, we have developed a number of strategies to determine four unknown beam parameters of interest: the two orthogonal beam divergences, δ' , ε' , which are perpendicular and parallel to the incidence plane, respectively, and the two corresponding orthogonal components of the beam size: δ , ε . These strategies require the measurement of the horizontally and vertically polarized intensities from a single slit or a double slit DR interferometer. We have demonstrated that one dimensional convolved scans of the horizontal intensities in either the $X = \text{const.}$ or $Y = \text{const.}$ plane can be used to separately measure δ' and ε' , respectively. With the divergences known, the corresponding beam size components δ and ε can be inferred. Since each of these scans can be produced at multiple angles in the plane of observation, a large amount of data is available which can be used to reduce the error in the measurement of all the beam parameters of interest. The strategies we have developed are useful for moderate to high energy lepton or hadron beams.

6 Appendix

To proceed to evaluate the integral presented in Eq. (1) we express $E_{ix}(x, y)$ by its Fourier transform, so that we have

$$E_x(k_x, k_y) = \frac{ie}{8\pi^4} \frac{1}{v} r_{\parallel}(\Psi) \iint \frac{k'_x}{(k'^2_x + k'^2_y + \bar{\alpha}^2)} e^{i(\vec{k}' - \vec{k}) \cdot \vec{\rho}} dk'_x dk'_y dx dy. \quad (16)$$

Here, $\bar{\alpha} \equiv 1/(\beta\gamma\bar{\lambda})$, and the phase term appearing in Eq. (16) above is

$$(\vec{k}' - \vec{k}) \cdot \vec{\rho} = (k'_x - \bar{k}_x)x' \sin \Psi + (k'_y - k_y)y' \quad (17)$$

where

$$\bar{k}_x \equiv k_x + (k_z - \vec{k}' \cdot \frac{\vec{v}}{v}) \cot \Psi. \quad (18)$$

Note that $\vec{k}' \cdot \vec{v} = \omega$, where ω is the frequency of the Fourier component of the field. This phase term takes into account the variation in phase with position $\vec{\rho}$ of the \vec{k}' Fourier component of the radiation field. For relativistic electrons, typically, $\gamma \gg 1$ and \vec{k}' is nearly along the direction Z in Fig. 1., which is the direction into which a ray along \vec{v} would be reflected if the screen were replaced by a mirror. The vector $\vec{k}' = \vec{k}_x + \vec{k}_y + \vec{k}_z \approx k(\theta_x \hat{x} + \theta_y \hat{y} + \hat{z})$ (see the x, y, z coordinate system in Fig. 1.), where $\theta^2 = \theta_x^2 + \theta_y^2$ and $\theta_x, \theta_y \ll 1$. For $\Psi = 45^\circ$, we have $\bar{k}_x \approx k(\theta_x - \gamma^{-2}/2) \approx k\theta_x$. Therefore, in general, the radiation pattern is shifted by an angle $\gamma^{-2}/2 \ll 1$.

The x and y integrations are straight forward. The variable y' ranges from $-\infty$ to a_1 and a_2 to $+\infty$, where the electron trajectory along \vec{v} is taken to be a distance a_1 from the lower edge and a distance a_2 from the upper edge of the slit so that $a = a_1 + a_2$ in Fig. 1. The x integration yields $2\pi\delta(k'_x - \bar{k}_x)$ so that the k'_x integral can be done trivially. Using $\bar{k}_x \approx k_x$, when $\gamma \gg 1$, we obtain

$$E_x(k_x, k_y) = \frac{ie}{2\pi^2} \frac{1}{v} r_{\parallel}(\Psi) \left\{ \frac{1}{2\pi} [I_1 + I_2] + \frac{k_x}{(k_x^2 + k_y^2 + \bar{\alpha}^2)} \right\} \quad (19)$$

where

$$I_1 = (-i) \int_{-\infty}^{+\infty} dk'_y \frac{k_x}{(k_x^2 + k_y^2 + \bar{\alpha}^2)} \frac{1}{k'_y - k_y} e^{-i(k'_y - k_y)a_1}, \quad (20)$$

and

$$I_2 = (+i) \int_{-\infty}^{+\infty} dk'_y \frac{k_x}{(k_x^2 + k_y^2 + \bar{\alpha}^2)} \frac{1}{k'_y - k_y} e^{i(k'_y - k_y)a_2}. \quad (21)$$

Now we can write

$$k_x^2 + k_y^2 + \bar{\alpha}^2 = (k'_y - if)(k'_y + if), \quad (22)$$

where

$$f^2 \equiv k_x^2 + \bar{\alpha}^2. \quad (23)$$

We see that I_1 and I_2 have poles at $k'_y = \pm if$, and at $k'_y = k_y$, where $I_1 = I_2^*(a_2 \rightarrow a_1)$. These integrals can be done using the contours shown in Fig. 14. The results are

$$I_1 = \pi \left\{ \frac{k_x}{f} \frac{1}{(f - ik_y)} e^{-a_1(f - ik_y)} - \frac{k_x}{(k_x^2 + k_y^2 + \bar{\alpha}^2)} \right\}, \quad (24)$$

and

$$I_2 = \pi \left\{ \frac{k_x}{f} \frac{1}{(f + ik_y)} e^{-a_2(f + ik_y)} - \frac{k_x}{(k_x^2 + k_y^2 + \bar{\alpha}^2)} \right\}. \quad (25)$$

Substituting these expressions for I_1 and I_2 into Eq. (19) above, one obtains Eqs.(2). Eq.(3), the expression for $E_y(k_x, k_y)$ can be derived in a similar manner. Note that when $a_{1,2} \rightarrow 0$, Eq. (19) gives the result for the transition radiation field as expected.

References

- [1] F. G. Bass, V. M. Yakovenko, Sov. Phys. Uspeki 8 (3) (1965), 420.
- [2] A. P. Kazantsev, G. I. Surdutovich, Sov.Phys. Dokl. 7 (1963) 990.
- [3] E. Keil, Nuc. Instrum. and Meth. 100 (1972), 419.
- [4] M. L. Ter-Mikaelian, High Energy Electromagnetic Processes in Condensed Media, Wiley-Interscience, New York, 1972.
- [5] N. J. Maresca and R. L. Liboff, Can. J. Phys. 53 (1975), 62.
- [6] Y. Shibata, et al., Phys. Rev. E 52 (1995), 6787.
- [7] I. Vnukov, et.al. JETP Letter, 67,(1998), 802.
- [8] A. P. Potylitsin, Nuc. Instr. and Meth. B, 145 (1998), 169.
- [9] M. Castellano, Nuc. Instr. Meth. A 394 (1997), 275.
- [10] D.W. Rule, R.B. Fiorito and W.D. Kimura, Nondestructive Beam Diagnostics Based on Diffraction Radiation, AIP Conf. Proc. 390, (1997), pp. 510-517 ; R. B. Fiorito, D. W. Rule and W. D. Kimura, Noninvasive Beam Position, Size, Divergence and Energy Diagnostics Using Diffraction Radiation, in CP472, *Advanced Accelerator Concepts: Eighth Workshop*, ed. W. Lawson, C. Bellamy and D. Brosius, AIP (1999), 725.
- [11] M.J. Moran and B. Chang, Nucl Instr. Meth. Phys. Res. B40/41, (1989), 970.
- [12] A. P. Potylitsin and N.A. Potylitsyna, Feasibility of Backward Diffraction Radiation for Nondestructive Beam Diagnostics of Relativistic Charge Particle Beams, Tomsk Polytechnic University, Tomsk, Russia, submitted to Phys. Lett.; arXiv, physics/0002034.
- [13] L. Wartski, et al., J. Appl. Phys.,46 (1975), 3644; L. Wartski, Ph.D.Thesis, Université de Paris-Sud, Centre d'Orsay, France (1976), unpublished.
- [14] R. B. Fiorito and D. W. Rule, OTR Beam Emittance Diagnostics, in Conf. Proc. No. 319 Beam Instrumentation Workshop, R. E. Shafer, ed., AIP (1994), 21.

FigureCaptions

Figure 1. A side view(1A), and a top view (1B), of backward diffraction radiation emitted by a charge passing through a slit which is oriented with its edge parallel to the plane of incidence (\mathbf{n}, \mathbf{v} plane).

Figure 2. A side view(2A), and a top view (2B), of backward diffraction radiation emitted by a charge passing through a slit which is oriented with its edge perpendicular to the plane of incidence (\mathbf{n}, \mathbf{v} plane).

Figure 3. Horizontal (3A) and vertical components (3B) of the intensity of DR for $R = a/\gamma\bar{\lambda} = 0.5$; the intensity (Z) axis is scaled in proportion to the corresponding intensity component of TR.

Figure 4. Horizontal (4A) and vertical components (4B) of the intensity of DR for $R = 2.0$; the intensity axis is scaled in proportion to the corresponding intensity component of TR.

Figure 5. Effect of the divergence δ' on the horizontal component of the intensity. Shown are line scans in the variable X for two values of the variable $Y = \delta' = 0.2$ and $Y = \delta = 0$, for a fixed value of the divergence $\varepsilon' = 0.1$ and $R = 2.0$.

Figure 6. Effect of divergence ε' on the horizontal intensity. Shown are line scans in the variable X for a fixed value of the beam size $\delta = 300\mu$ and $R = 2$.

Figure 7. Effect of beam size δ on the horizontal intensity. Shown are line scans taken in the X, Z plane, i.e. $Y = 0$, for a fixed value of divergence $\varepsilon' = 0$ and $R = 2.0$.

Figure 8. Effect of the beam divergence ε' on the vertical intensity. Shown are line scans in the variable Y for two values of the variable $X = \varepsilon' = 0.2$ and $X = \varepsilon' = 0$, for a fixed value of the divergence $\delta' = 0.1$, and $R = 2$.

Figure 9. Effect of divergence δ' on the vertical intensity. Shown are line scans taken at $X = 0$ for a fixed value of the beam size, $\delta = 200\mu$ and $R = 2.0$.

Figure 10. Effect of beam size δ on the vertical intensity. Shown are line scans taken at $X = 0$ for a fixed value of the divergence, $\delta' = 0$ and $R = 2.0$.

Figure 11. Configuration of a DR interferometer composed of two slits oriented with the edges parallel to the plane of incidence.

Figure12. Vertical component of intensity from a DR interferometer for an electron beam with energy $E = 500$ MeV; $R = 2$, $\lambda = 3.2\mu m$, $\delta = 200\mu$, $\delta' = 0.05$ and separation distance $L = 6L_v = 3$ meters.

Figure13. Horizontal component of intensity from a DR interferometer for an electron beam with same parameters as in Fig. 12.

Figure 14. Contours used to evaluate the integrals I_1 and I_2 defined by Eqs. (20) and (21), respectively.

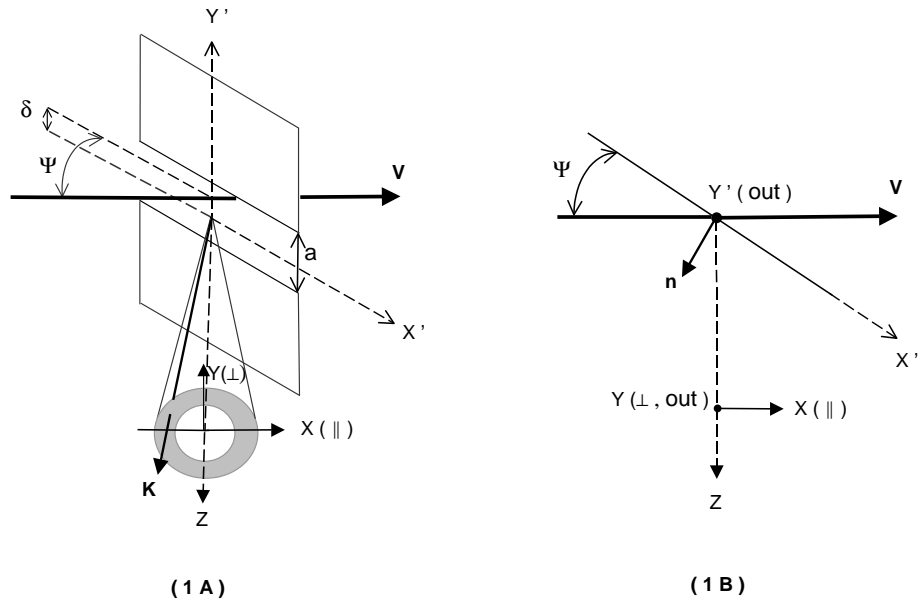


Figure 1

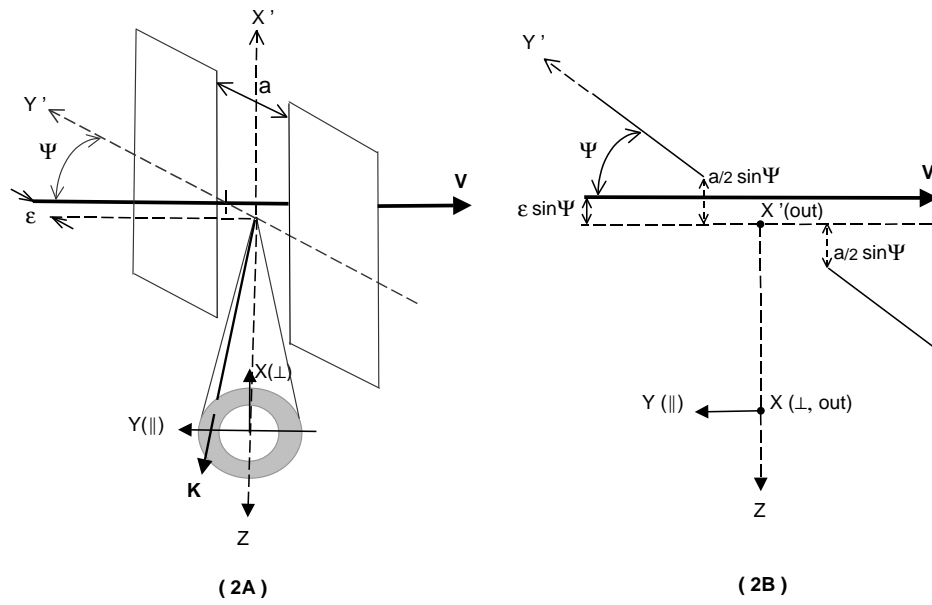


Figure 2

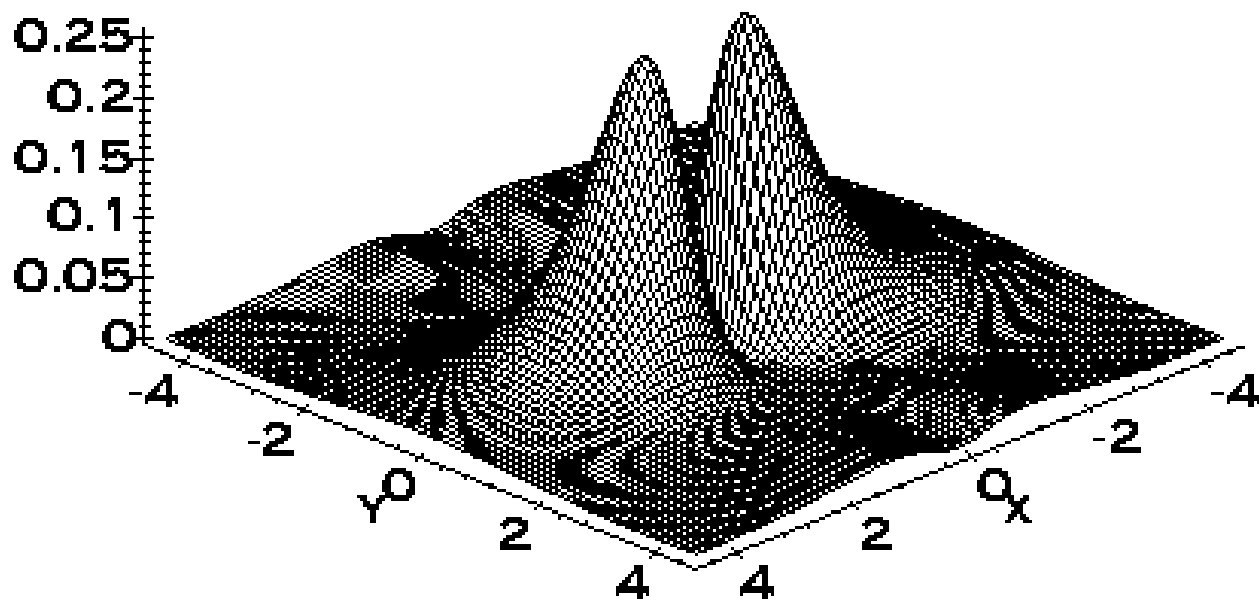
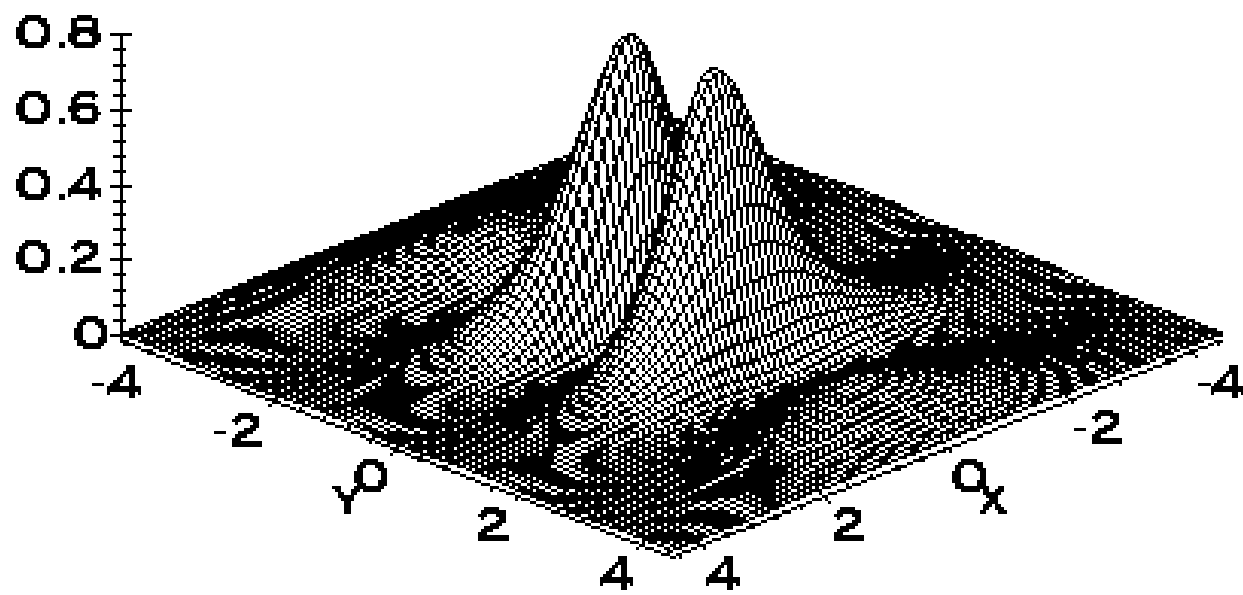


Figure 3A



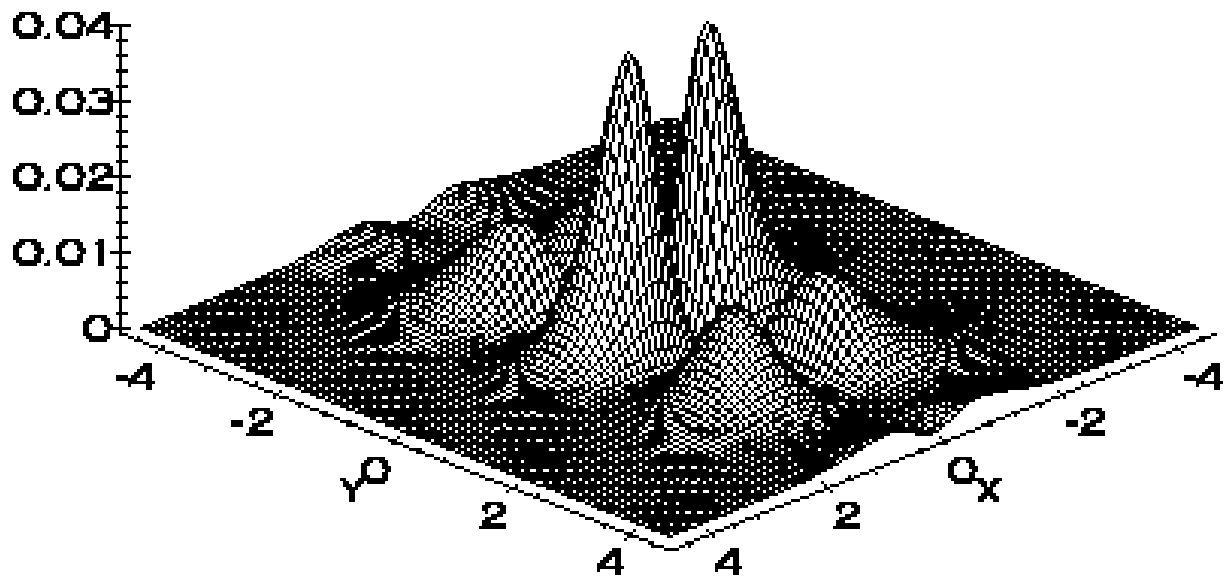


Figure 4A

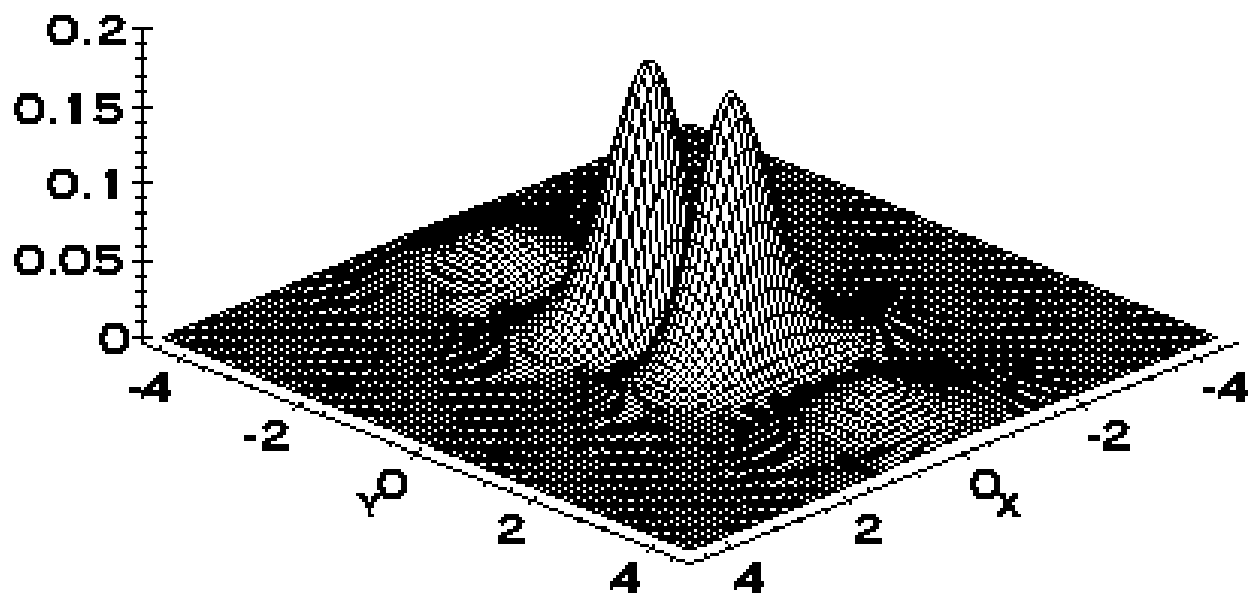


Figure 4B

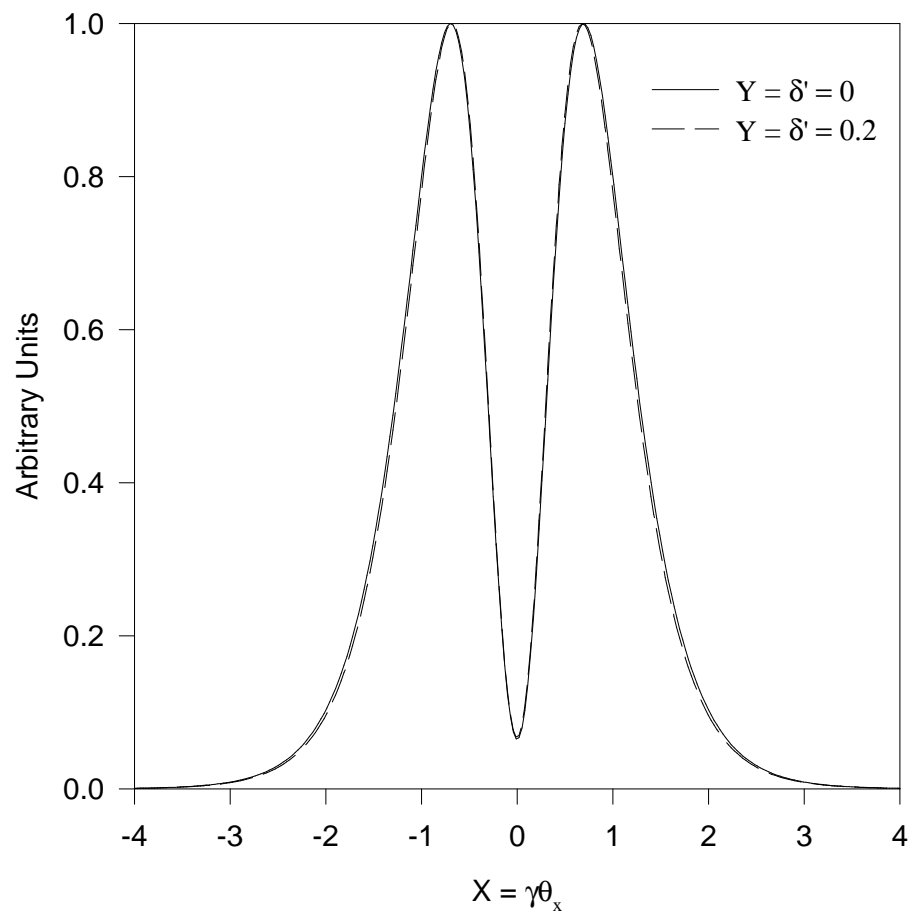


Figure 5

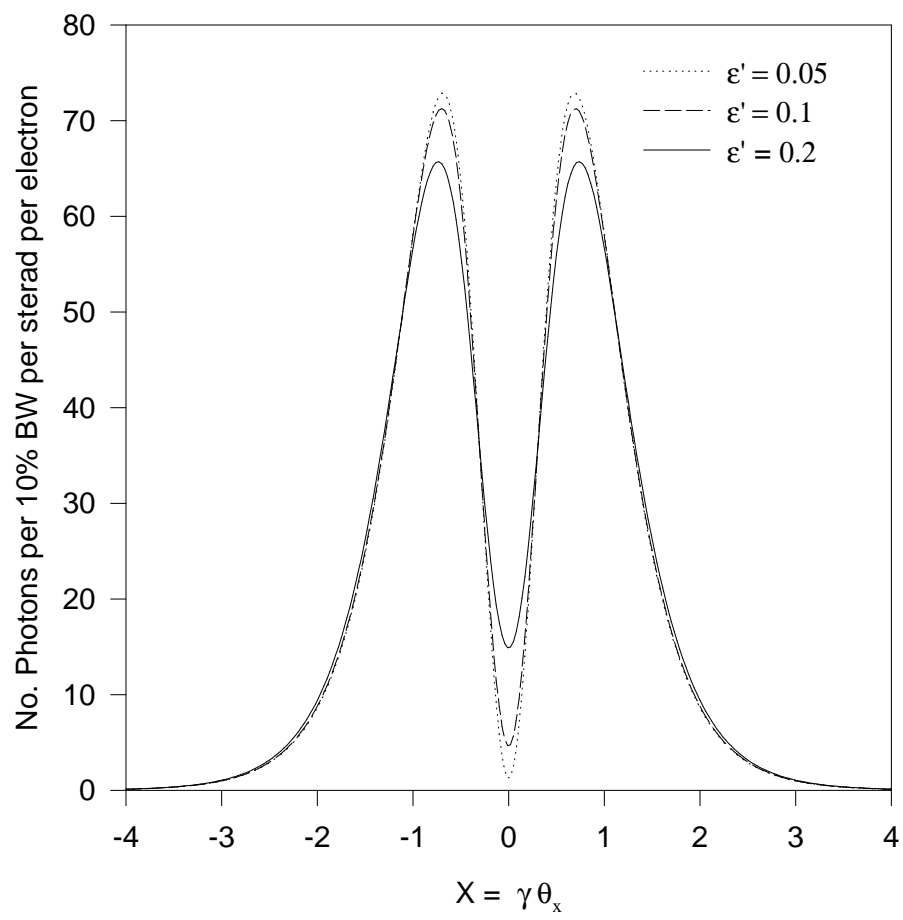


Figure 6

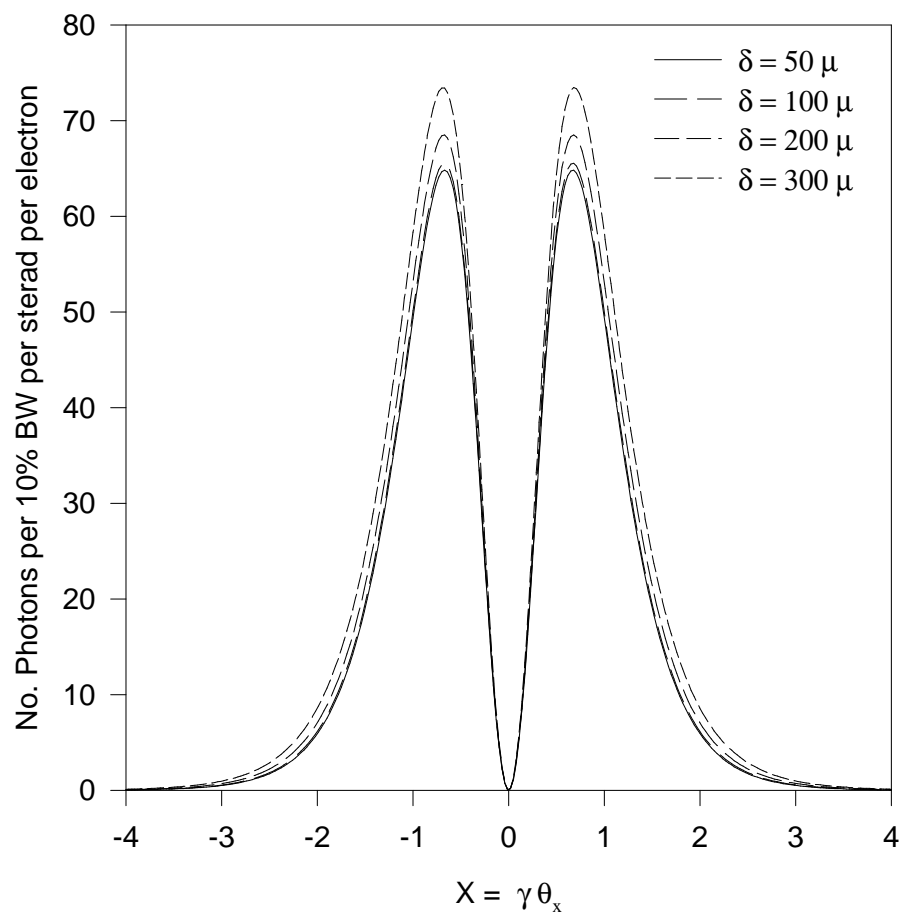


Figure 7

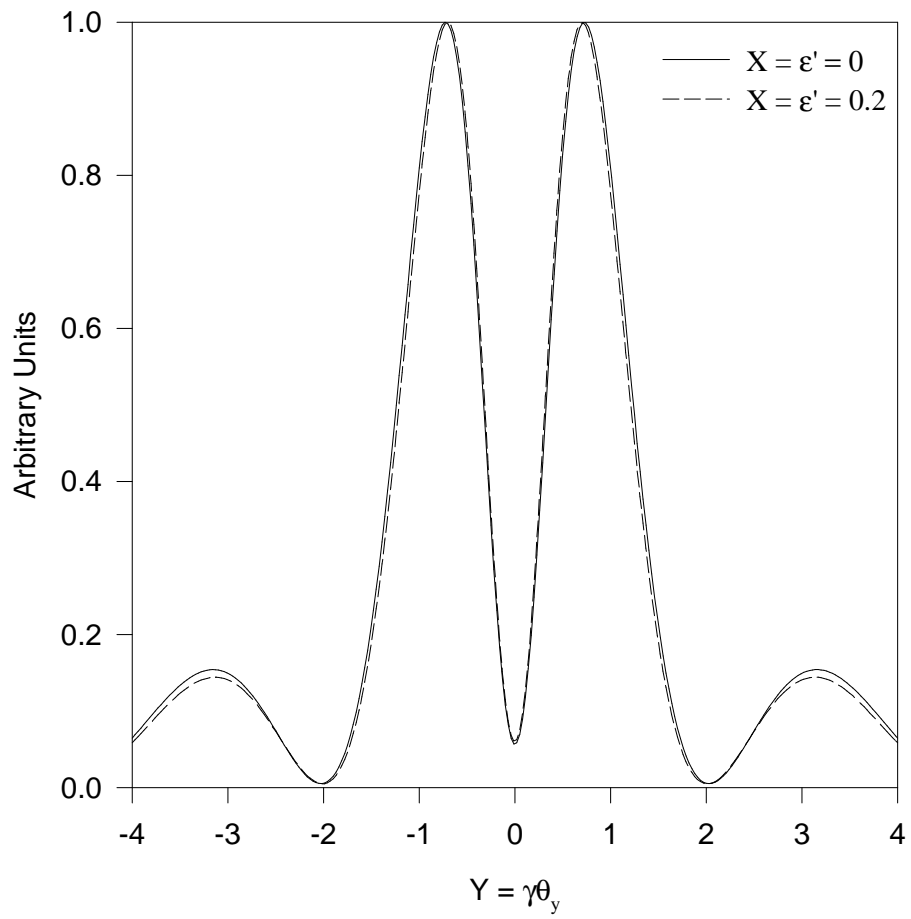


Figure 8

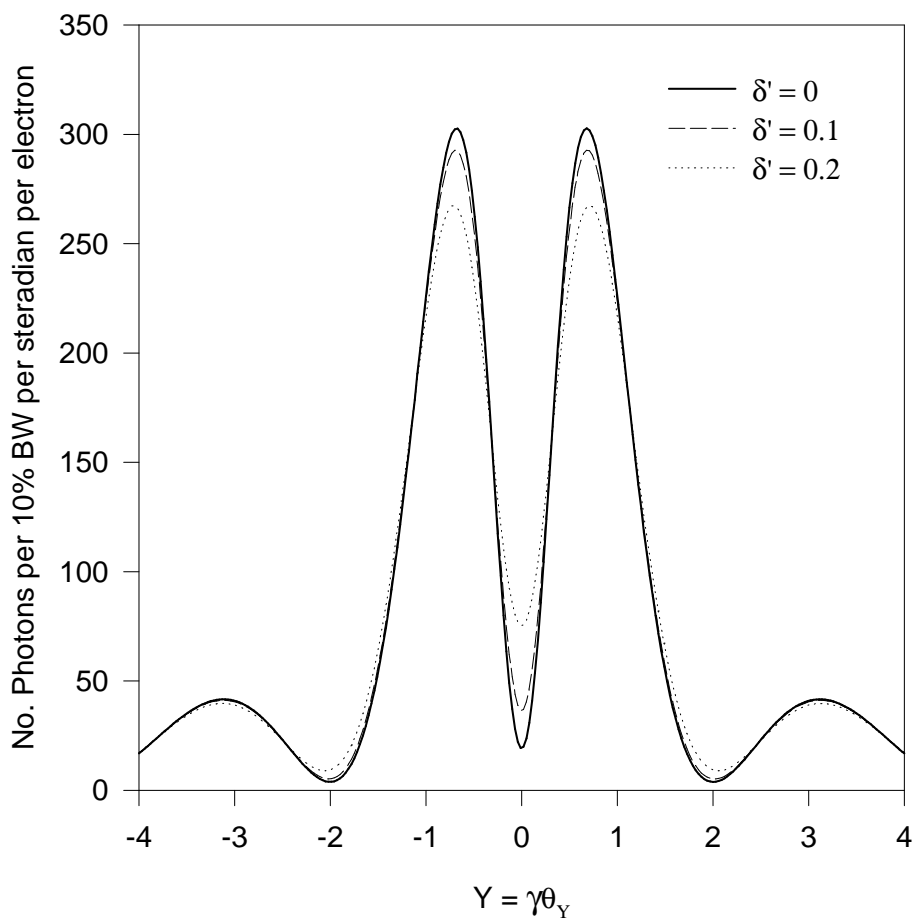


Figure 9

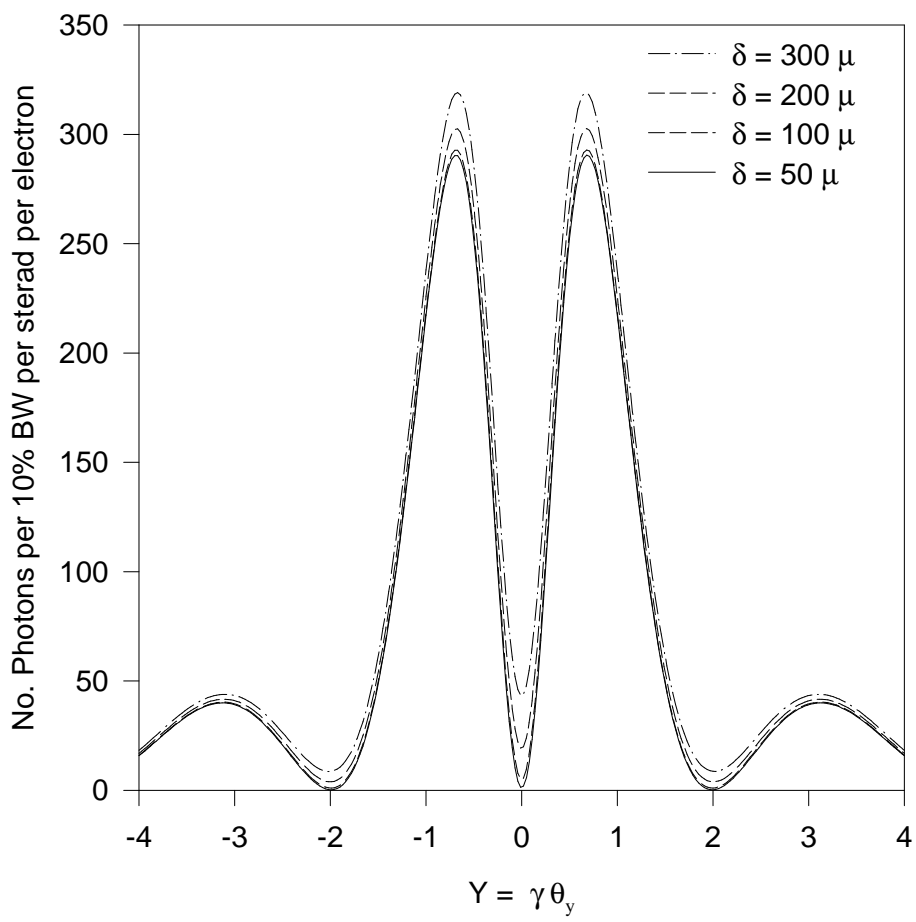


Figure 10

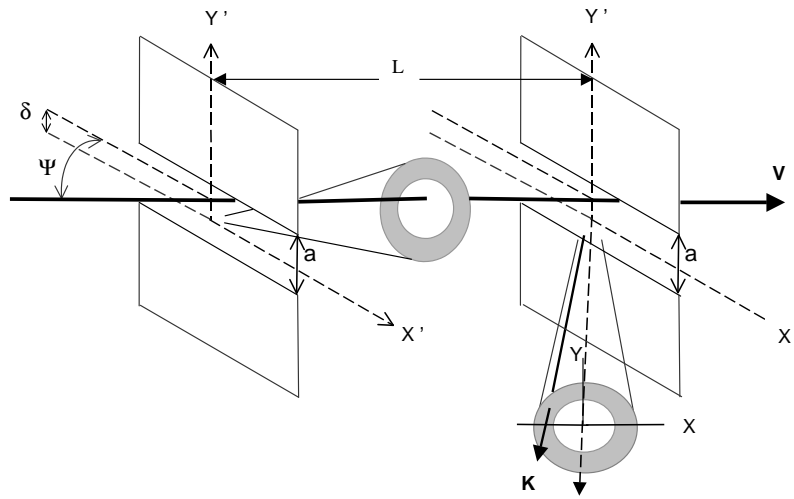


Figure 11

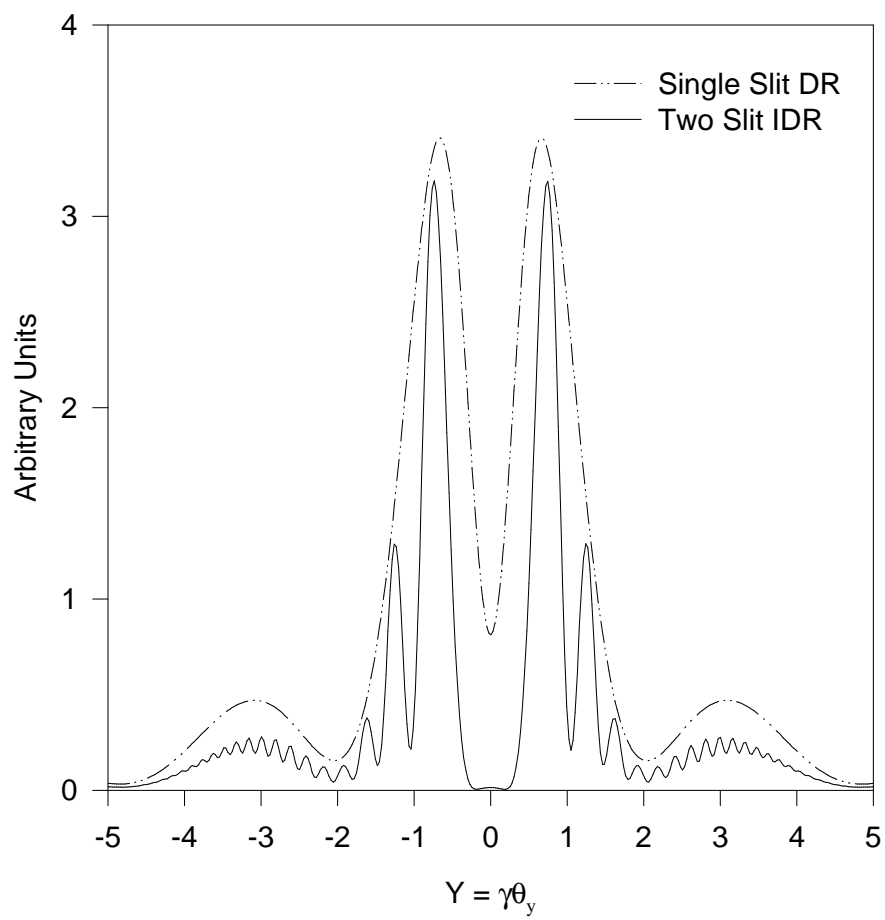


Figure 12

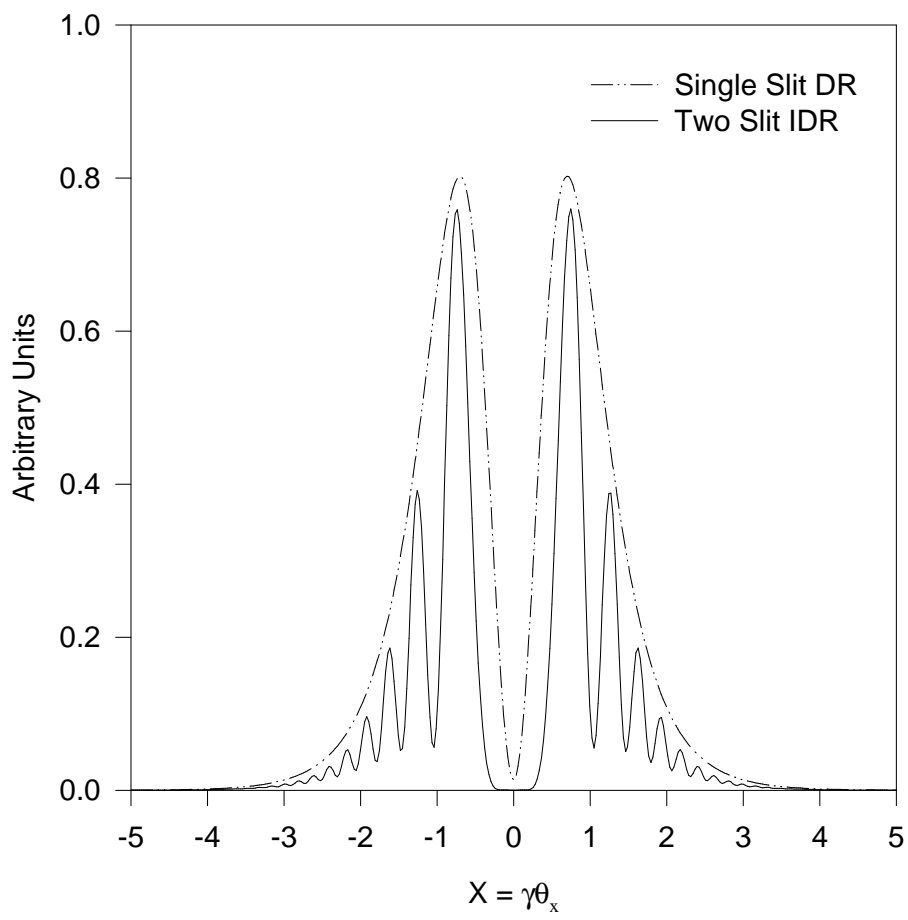


Figure 13

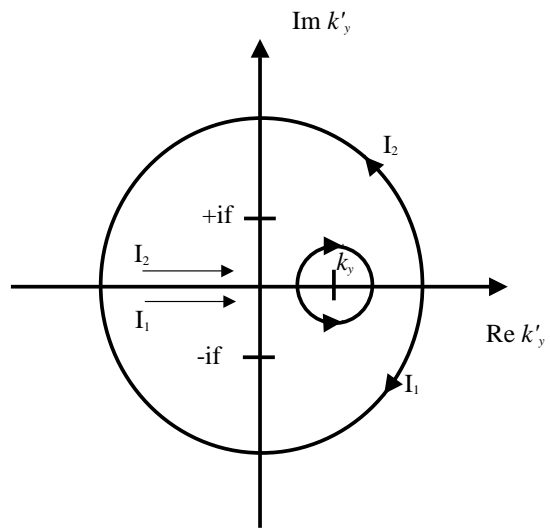


Figure 14